Toward a numerical deshaker for PFS

F. Schmidt [a,b,*], I. Shatalina [c], M. Kowalski [d], N. Gac [d], B. Saggin [c], M. Giuranna [e]

[a] Univ. Paris-Sud, Laboratoire IDES, UMR 8148, Bât 509, Orsay, F-91405, France
[b] CNRS, Orsay, F-91405, France
[c] Dipartimento di Meccanica, Politecnico di Milano, Campus of Lecco, Via M. d'Oggiono 18/a, 23900, Lecco, Italy
[d] Laboratoire des signaux et systemes (L2S), UMR8506 Univ Paris-Sud- CNRS – SUPELEC, SUPELEC, 3 rue Joliot Curie, Gif sur Yvette, F-91192, France
[e] IFSI, via del Fosso del Cavaliere, 100, 00133 Roma, Italy

Article history:
Received 3 April 2013
Received in revised form
14 November 2013
Accepted 27 November 2013
Available online 18 December 2013

1. Introduction

The Planetary Fourier Spectrometer (PFS) is a double pendulum Fourier transform infrared spectrometer instrument onboard MEx, operating in the 1.2–5.5 μm for the Short Wavelength Channel (SWC), and 5–45 μ in the Long Wavelength Channel (LWC) (Formisano et al., 2005). It is based on a modified Michelson's scheme using a double pendulum with cubic reflectors. The optical path difference is defined by the zero crossing of a laser tacking the same optical path as the signal. The spectra presented in this article are the numerical Fourier transform of the recorded interferograms.

An experimental study of mechanical vibration impact on Fourier-transform spectrometer has been proposed based on PFS example (Comolli and Saggin, 2005). Analytical expression of all distortion effects have been formulated separately (Saggin et al., 2007): offset of the reference laser signal, mirrors speed variation, periodic misalignments, detector nonlinearity and internal reflections. More recently, a numerical simulation model has been proposed to explore all effects combined in order to understand the PFS signal (Comolli and Saggin, 2010). Perturbations are creating artificial features, called "ghosts", present in some spectra of the SWC but not in the LWC, thanks to the optimization of the pendulum velocity (Giuranna et al., 2005a, 2005b). Since the amplitude of ghosts is small (few % of the original signal) and its phase has a stochastic behavior, the worst cases correspond to only few significant ghosts (Shatalina et al., submitted for publication).

Quantitatively, the ghosts are affecting few % of the total spectrum energy (3% typically; 5% maximum). When single spectra are used, the absolute radiometric calibration is degraded, and spurious spectral features may appear in the spectrum, preventing any surface-related analysis, and introducing possible large uncertainties in the quantitative retrievals of abundances of minor species in the atmosphere. When discussing the calibration procedure for the SWC (Giuranna et al., 2005b) and the LWC (Giuranna et al., 2005a), the authors suggest to stack the data to correct for the effects of the mechanical vibrations. The position of ghosts depends on the frequencies of the external vibrations, which have been found to be quite stable. Since the phase of ghosts is random and the external frequencies are stable, only the signal should be coherent during the stack. This idea has been confirmed by numerical modeling of the perturbations (Comolli and Saggin, 2010). Practically, averaging a few spectra (ten or so) is enough to average out the ghosts. However, this will degrade the spatial and temporal resolution of PFS measurements, limiting the interpretation of small-scale features and hampering some scientific studies (e.g., the composition of ices; detection of minerals at the surface).

Typical PFS raw measurements are shown in Fig. 1. One can identify the major signals from Mars: thermal emission and

* Corresponding author.
E-mail address: frederic.schmidt@u-psud.fr (F. Schmidt).

reflection of solar energy, and the laser line stray-light. Also the contribution due to mechanical vibrations is shown on the signal, leading to additional energy shifted on left and right almost symmetrically. The ghost of the laser line is only one sided due to aliasing.

Our aim is to provide a new approach to process the PFS instrument with following constraint:

1. Correct the effect of mechanical vibrations due to both misalignment and optical path difference errors.
2. Perform the correction on each spectrum separately.
3. Validate the approach by using actual PFS observations.

In order to avoid unphysical solution, the algorithm is initialized with an a priori guess of the large scale structure of the spectra, adapted to each measurement, reproducing the Martian thermal emission and the reflected solar light (see Section 2.2.2).

A check of the correction can be done but requires the SWC laser diode switched on to estimate the vibration kernel independently (see Section 2.3).

2. Method

This section describes the direct model of the Martian spectra affected by vibrations. Then, an iterative procedure is exposed in order to invert it as well as some criteria to measure the quality of our estimation.

2.1. Analytical formulation in the signal domain (0–5000 cm^{-1})

As it can be seen from Fig. 1, it is possible to separate the whole spectrum into two wavenumber domains to deal the effects of the mechanical vibrations apart in each of them. From 0 to 5000 points (5000∗1.02 cm^{-1}), we define the signal domain, where the thermal energy from Mars and the most of the reflected Martian

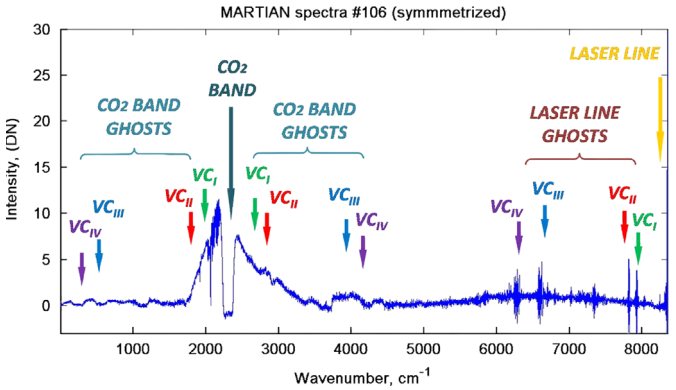

Fig. 1. Typical symmetrized PFS measurement in SWC. Signal and major CO_2 band and laser lines are noted. The four main ghosts are identified as "Vibration Component" (VC) affecting both signal and laser line.

energy are recorded, without significant laser line artefacts. The laser line domain is defined from 5000 cm^{-1} to 8330 cm^{-1}. It contains also the Martian signal but affected by laser line artefacts. Below 1700 cm^{-1} there is no meaningful signal due to the low detector responsivity (see Fig. 15 in Giuranna et al., 2005b), and this region is characterized only by ghosts of the continuum.

At larger wavenumber than 5000 cm^{-1}, the signal is affected by the laser line shape and its ghosts, directly and in aliasing. This domain will be used to test the coherence of the results. Since the laser has been switched off after orbit 634, it could not be used for the complete PFS archive (see Section 2.3).

Using some mathematical reorganization and simplification, the analytical expression of mechanical vibration due to periodic misalignment and optical path errors can be written as a convolution products in complex form, see Eq. (13) in Shatalina et al. (submitted for publication). Assuming that the domain of wavenumber with significant signal I_{Mars} around $\sigma \sim 2000$–3000 cm^{-1} is constant ($\sigma_k \sim 2500$), the following equation

$$I_{PFS}(\sigma) = I_{Mars}(\sigma) + [\sigma . I_{Mars}(\sigma)] \star K(\sigma), \quad (1)$$

simplifies to

$$I_{PFS}(\sigma) = I_{Mars}(\sigma) \star [\delta(\sigma) + K(\sigma).\sigma_k]. \quad (2)$$

with $\delta()$, the Dirac function.

By rewriting

$$I_{PFS}(\sigma) = I_{Mars}(\sigma) \star K_{PFS}(\sigma), \quad (3)$$

with $I_{PFS}(\sigma)$ the measured raw spectra, I_{Mars} the contribution of the raw spectra from Mars, K_{PFS} the kernel representing the mechanical vibration effects, σ the wavenumber, and $K(\sigma)$ the non-normalized complex kernel (Shatalina et al., submitted for publication).

From Shatalina et al. (submitted for publication), the kernel of all frequency of vibrations is

$$K_{PFS}(\sigma) = \delta(\sigma) + A(\sigma) e^{i\varphi_A(\sigma)} + B(\sigma) e^{i\varphi_B(\sigma)}. \quad (4)$$

The quantities A, B, φ_A, φ_B are unknown and cannot be evaluated quantitatively due to the lack of knowledge about vibration amplitude and phase. In practice, the functions A, B, φ_A, φ_B are sparse over σ because the frequencies of vibrations are sparse. Note that A, B, φ_A, φ_B are not symmetric around $\sigma = 0$ due to the relative phase. We propose to estimate those functions using an inversion procedure described in the next section.

The assumption of a reduced wavenumber domain is valid in first approximation due to the sensitivity of the detector and the typical Martian signal, leading to a misfit factor of 0.8 × to 1.2 × that is reasonable for this case. In addition, our strategy is to use semi-blind deconvolution algorithm in order to ensure the best fit any kind of spectra. This way, the wavenumber domain of significant signal has not to be defined explicitly.

Including to our model an additive noise ε which stands for the others sources of acquisition noise besides the mechanical vibrations and the error due to our PFS modeling by a convolution kernel K_{PFS}, PFS spectra in signal domain as illustrated in Fig. 2 are

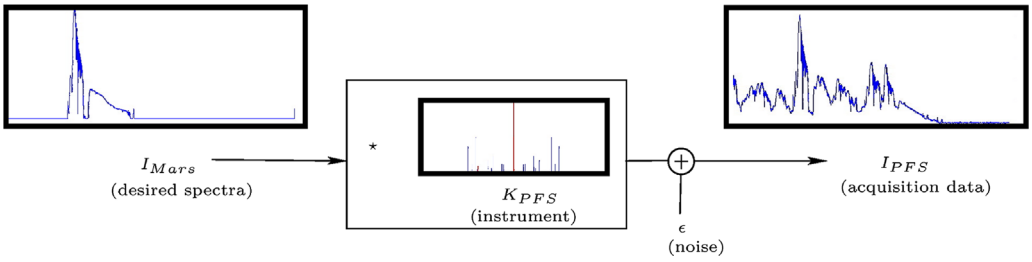

Fig. 2. Model of acquisition by the PFS instrument.

obtained through

$$I_{PFS}(\sigma) = I_{Mars}(\sigma) \star K_{PFS}(\sigma) + \varepsilon. \quad (5)$$

2.2. Inversion

From the direct model of the PFS instrument described above, see Eq. (5), we propose here a semi-blind deconvolution method to solve the inverse problem: estimation of the desired spectra I_{Mars} from the PFS spectra I_{PFS} although the convolution kernel K_{PFS} is unknown. We qualified our method as semi-blind because the only spectral a priori information is $\hat{I}^0_{Mars}$, known as ab initio. We also used two a priori information: $\hat{I}_{Mars}$ is smooth and $\hat{K}_{PFS}$ is sparse. The notation, $\hat{X}$, means the estimation of quantity X. A classical approach consists in introducing a cost function $\mathcal{C}$ whose minimum provides an estimation:

$$\begin{aligned}\hat{I}_{Mars}, \hat{K}_{PFS} &= \arg \min_{I_{Mars}, K_{PFS}} \mathcal{C}(I_{Mars}, K_{PFS}) \\ &= \arg \min_{I_{Mars}, K_{PFS}} \frac{1}{2} \| I_{PFS} - K_{PFS} \star I_{Mars} \|_2^2 + \lambda_K \| K_{PFS} \|_1 + \frac{\lambda_{Mars}}{2} \| D \star I_{Mars} \|_2^2. \end{aligned} \quad (6)$$

Three terms appear in $\mathcal{C}$:

1. A data fit term $\frac{1}{2} \| I_{PFS} - K_{PFS} \star I_{Mars} \|_2^2$ that quantifies how well the estimated sources match the measured data. This term takes into account the characteristics of the noise supposed to be white and Gaussian. This data match term is sensitive to high frequency noise and must be balanced with regularization term which corresponds to a mathematical prior on the expected solution (Idier, 2008).
2. A sparsity regularization term $\| K_{PFS} \|_1$ is chosen for the kernel, i.e., the ℓ_1 norm (sum absolute value) of the kernel must be low. Indeed, the PFS kernel is supposed to be composed with few Diracs at mechanical vibration frequencies.
3. A smooth regularization term is chosen for the Mars spectra: $\| D \star I_{Mars} \|_2^2$, where D is a discrete first-order derivation operator. This prior promotes smooth solution in order to avoid noise improvement.

All these terms are balanced with two hyperparameters λ_K and λ_{Mars} , both positive. The functional (6) is convex for each variables – convex in I_{Mars} when K_{PFS} is fixed and vice versa – but not from the couple (I_{Mars}, K_{PFS}). The strategy we choose here is a classical alternative procedure: from initial guesses $\hat{I}^0_{Mars}$, an iterative procedure updates successively at each iteration n, the new estimates $\hat{K}^{n+1}_{PFS}$ and $\hat{I}^{n+1}_{Mars}$. (Fig. 3)

2.2.1. Iterative procedure

At each iteration n we estimate successively the kernel $\hat{K}^{n+1}_{PFS}$ and the signal $\hat{I}^{n+1}_{Mars}$ until iteration N using the following steps:

1. First estimation of the kernel $\hat{K}^1_{PFS}$ from filtered $\hat{I}^0_{Mars}$ and I_{PFS} with L1 regularization.
2. Iterative loop:
   (a) estimation of the Mars spectra $\hat{I}^{n+1}_{Mars}$ from unfiltered $\hat{K}^n_{PFS}$ and I_{PFS} with smooth regularization,
   (b) estimation of the kernel $\hat{K}^{n+1}_{PFS}$ from unfiltered $\hat{I}^{n+1}_{Mars}$ and I_{PFS} with L1 regularization.
3. Last estimation of the Mars spectra $\hat{I}^{final}_{Mars}$ from unfiltered $\hat{K}^{final}_{PFS}$ and I_{PFS}.

For both estimations, a convex optimization algorithm converges to the solution defined by the minimum of a criteria made of a data match and a regularization terms. This means that the solution is unique and can be estimated either analytically or iteratively.

Since the first step of the iterative procedure is the estimation of the kernel $\hat{K}^1_{PFS}$, the only a priori information of this iterative procedure, $\hat{I}^0_{Mars}$, estimated ab initio. Since $\hat{I}^0_{Mars}$ can only be estimated at large scale (all absorption lines may differ from spectra to spectra due to non-homogeneity of chemical compounds in the atmosphere/surface of Mars), the first iteration is done in a low-pass filtered space, as described in Section 2.2.2.

Estimation of the PFS kernel: The estimation of the PFS kernel reduce to the following ℓ_1 regularized convex (non-smooth) problem:

$$\hat{K}^{n+1}_{PFS} = \arg \min_{K_{PFS}} \frac{1}{2} \| I_{PFS} - K_{PFS} \star \hat{I}^n_{Mars} \|_2^2 + \lambda_K \| K_{PFS} \|_1, \quad (7)$$

where $\hat{I}^n_{Mars}$ is the estimation of the Mars spectra at the iteration number n. This problem is the well known Lasso (Tibshirani, 1996) or Basis-Pursuit Denoising (Chen et al., 1998) problem, and can be solved efficiently with the Fast Iterative/Thresholding Algorithm (FISTA) (Beck and Teboulle, 2009). Denoting by $\tilde{I}$ the adjoint of the kernel I and by S_λ the so-called soft-thresholding operator[1] the algorithm reads as follows:

1. Let $i = 0,\ \tau^0 = 1,\ k = 1,\ Z_0 = K^n_{PFS}$ and $L = \| I_{Mars} \|^2$.
2. $K^i_{PFS} = S_{\lambda_K / L}(Z^i + \frac{1}{L}(I_{PFS} - Z^i \star \hat{I}^n_{Mars}) \star \tilde{\hat{I}}^n_{Mars})$
3. $\tau^{i+1} = \frac{1 + \sqrt{1 + 4\tau^{i2}}}{2}$
4. $Z^{i+1} = K^i_{PFS} + \frac{\tau^i - 1}{\tau^{i+1}}(K^i_{PFS} - K^{i-1}_{PFS})$
5. $i = i + 1$
6. Go to 2 until $i = i_{max}$
7. $K^{n+1}_{PFS} = K^{i_{max}}_{PFS}$

From theoretical consideration, the kernel K_{PFS} must be a Dirac-shape on zero, so we concentrate the energy around zero into a Dirac to create the kernel estimation $\hat{K}^n_{PFS}$. We would like to emphasize that there is no analytical solution of Eq. (7) so we solve this equation with an iterative procedure, initialized with the previous step K^n_{PFS}. For the first initialization K^0_{PFS}, we may use $\hat{K}^{approx}_{PFS}$ but any other guess (such zero) may apply when the laser line has been switch off. Nevertheless, closer the initialization, faster the convergence.

Estimation of the Mars spectra: For the Mars spectra, the estimation reduces to a classical Thikonov regularization (Idier, 2008):

$$\hat{I}^{n+1}_{Mars} = \arg \min_{I_{Mars}} \| I_{PFS} - \hat{K}^{n+1}_{PFS} \star I_{Mars} \|_2^2 + \lambda_{Mars} \| D \star I_{Mars} \|_2^2 \quad (8)$$

Thanks to the fact that a convolution is diagonal in the Fourier domain, and the Parseval theorem, the solution reads as follows:

$$\begin{aligned}\mathcal{F}(\hat{I}^{n+1}_{Mars}) = \arg \min_{\mathcal{F}(I_{Mars})} & \| \mathcal{F}(I_{PFS}) - \mathcal{F}(\hat{K}^{n+1}_{PFS}) \odot \mathcal{F}(I_{Mars}) \|_2^2 \\ & + \lambda_{Mars} \| \mathcal{F}(D) \odot \mathcal{F}(I_{Mars}) \|_2^2 \end{aligned} \quad (9)$$

where $\odot$ is the Hadarmard element-wise product and $\mathcal{F}$ the Fourier transform. Then, the estimation of the Mars spectra at iteration $n+1$ is given in close form by

$$\hat{I}^{n+1}_{Mars} = \mathcal{F}^{-1}(\mathcal{F}(I_{PFS}) \odot (\mathcal{F}(\hat{K}^{n+1}_{PFS})^{-2} - \lambda_{Mars} \mathcal{F}(D)^{-2})), \quad (10)$$

where $\mathcal{F}(\hat{K}^{n+1}_{PFS})^{-2}$ (resp. $\mathcal{F}(D)^{-2}$) represents the vector containing the inverted squared elements of the vector $\mathcal{F}(\hat{K}^{n+1}_{PFS})$ (resp. $\mathcal{F}(D)$).

We would like to emphasize that Eq. (10) is the analytical solution of Eq. (8) that did not require initialization.

[1] $S_\lambda(x) = x/|x| \max(|x| - \lambda, 0)$

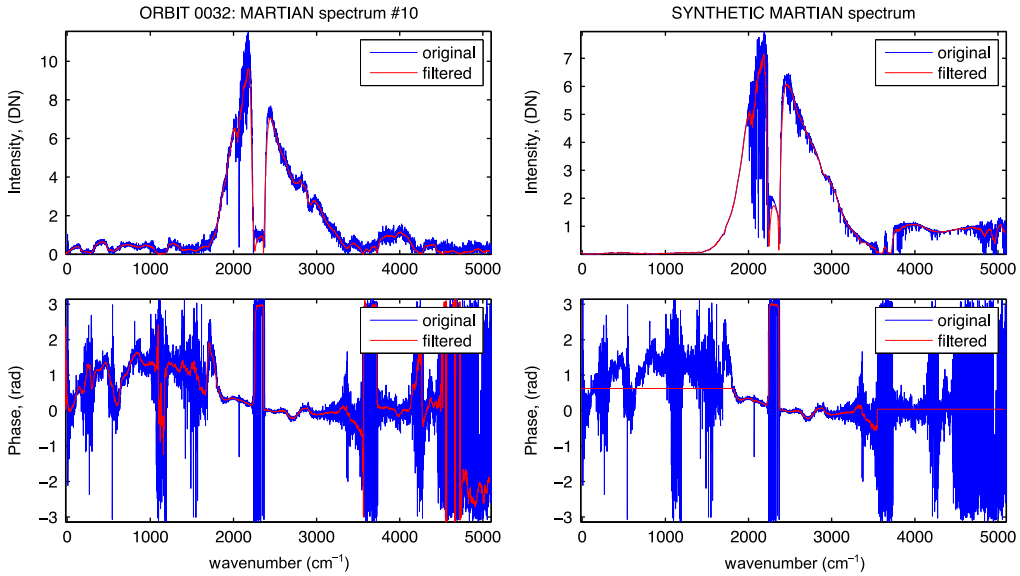

Fig. 3. Raw measurements I_{PFS} (on left) and initial guess of the Martian signal $\hat{I}^0_{Mars}$ (on right) for the PFS measurement ORB0032, No. 106.

2.2.2. Initial guesses of the Martian spectra and PFS kernel

Initial Mars spectra guess: We estimate the Martian spectra large scale feature (noted $\hat{I}^0_{Mars}$) by two Planck functions and the major absorption feature, representing (i) the Martian thermal emission and (ii) the solar energy reflected back by Mars and (iii) the 2200–2400 cm^{-1} gap, representing the CO_2 absorption band. The Martian temperature is estimated by fitting the 2500–3000 cm^{-1} domain, where the ghost seems to be less pronounced. The Planck function of the sun is scaled to the 3800–4200 cm^{-1} domain. We derive the raw spectra using the calibrations of detector responsivity and deep space measurements (Giuranna et al., 2005b). This initial guess is only valid at large scale because the absorption lines of major and minor gases may change due to local pressure, atmospheric circulation, surface change and radiative transfer effects.

The phase of the initial guess is taken similar to the signal in the domain where the ghosts are absent and a constant extrapolation is proposed to the ghosted region.

Because the iterative procedure is sensitive to initialization, both PFS spectra I_{PFS} and mars initial guess $\hat{I}^0_{Mars}$ are filtered with a low-pass filter with a cut off frequency of $1/20\Delta\sigma$, where $\Delta\sigma = 1.02$ cm^{-1} is the spectral resolution, in order to keep the realistic features.

The initial guess $\hat{I}^0_{Mars}$ will force the initial step of the iterative procedure to find a local minimum around physical solution. Initializing the procedure with random or constant signal leads to non-physical solutions.

Initial PFS Kernel guess: Thanks to the approximation from Shatalina et al. (submitted for publication), an estimation of the kernel $\hat{K}^{approx}_{PFS}$ from the laser line domain can be done (see Section 2.3). Neither amplitudes nor phases are precise but the frequencies should be well described by this methodology. This kernel is used as initial guess $\hat{K}^0_{PFS}$ to reach faster the convergence of the first kernel estimation $\hat{K}^1_{PFS}$. Unfortunately, only Mars Express orbits <634 are usable for this estimation. It represents 310 orbits out of 6255 orbits currently available, i.e., less than 5% of the total current orbits.

2.3. Laser line domain (5000–8330 cm^{-1})

Knowing that laser line is almost Dirac shaped, we could first hypothesize that the kernel K_{PFS} can be directly measured in the laser line domain. Unfortunately due to aliasing (laser line ghosts from left and right are superposed), from $I_{PFS}(\sigma)$ it is not possible to realize an inversion to estimate K_{PFS} because there are twice unknown variables in comparison to known variable. Under strong hypothesis, it is possible to estimate an approximation of $\hat{K}^{approx}_{PFS}$ (Shatalina et al., submitted for publication).

Nevertheless, the recent analytical formulation of the mechanical effects on the laser line allows us to compute the exact effect of the mechanical vibration on the laser line, knowing the vibration kernel K_{PFS} (see complex expression in Shatalina et al., submitted for publication). After the estimation of K_{PFS}, one simple test of coherence would be to compare the observed laser line ghost to the one predicted.

2.4. Quality of the results

We propose several criteria to estimate if the deconvolution is correct.

2.4.1. Distance between real and simulated PFS spectra

Because the only ground truth we could have is the real PFS spectra I_{PFS}, it should be as close as possible to the final simulated PFS spectra $\hat{I}^{final}_{PFS} = \hat{I}^{final}_{Mars} \star \hat{K}^{final}_{PFS}$. We use the Root Mean Square distance (RMS) of $\hat{I}^{final}_{PFS} - I_{PFS}$. In this way, we evaluate at the same time the correctness of the estimated Mars spectra $\hat{I}^{final}_{Mars}$ and the instrument model $\hat{K}^{final}_{PFS}$.

2.4.2. Ghost removal in the signal domain (1–5000 cm^{-1})

In the 1–1530 cm^{-1} wavenumber domain, no signal is expected due to the very low signal to noise ratio but only the ghosts are present in the raw spectra. Thus, one simple criterion to estimate the efficiency of the correction is to measure the energy in this domain.

2.4.3. Ghosts in the laser line domain (5000–8330 cm^{-1})

The laser line modulated $\hat{I}^{final}_{LM}$ through filter, aliasing and vibrations effects can be computed from the estimated kernel $\hat{K}^{final}_{PFS}$ using the exact formulation of Shatalina et al. (submitted for publication). To check the quality of the results, we evaluate the distance between the actually measured signal and the predicted laser line modulated with its ghosts.

2.4.4. Distance to the approximated kernel

The estimation of the kernel $\hat{K}_{PFS}^{approx}$ from the laser line domain can be done. Neither amplitudes nor phases are precise but the frequencies should be well described by this methodology. The distance between $\hat{K}_{PFS}^{approx}$ and $\hat{K}_{PFS}^{final}$ is also a criteria of good results.

2.4.5. Comparison with vibration frequencies from MEx telemetry and technical specification

Several sources of vibrations are present in the MEx platform, mainly reaction wheels, Inertia Measurement Unit (IMU) dithering. PFS eigenmodes can also be exited and are considered as "source" of vibrations. Since, these vibrations are not unique onboard MEx (cryocooler, other instruments, etc.) and the uncertainties on these vibrations frequencies are not known, it is not possible to have a supervised approach. One also has to note that all vibration frequencies may not be present in a PFS spectrum, depending on the coupling with PFS. Nevertheless, a comparison between our blind estimation and the actual data is interesting.

From each vibration frequency f_d (in Hz), the perturbation is at wavenumber $\sigma = f_d/v_m$ (Saggin et al., 2007; Shatalina et al., submitted for publication), with the pendulum speed $v_m = d_{zc} f_{zc}$ where the zero-crossing frequencies f_{zc} is 2500 Hz and zero-crossing length d_{zc} is 1.2 μ for typical PFS measurements at Mars (Giuranna et al., 2005b).

Reaction wheels: Thanks to telemetry data from ESA, it is possible to estimate the frequencies of reaction wheels for ORB0032, spectra No. 106 at 56.7 Hz, 33.3 Hz, 40.6 Hz and 30.3 Hz. Uncertainties are unknown and those frequencies of micro-vibrations are expected to change during the mission but can be estimated from telemetry.

IMU: Astrium technical specification of MEx (MEX.MMT. HO.2379) states that the IMU dithering onboard MEx is at 513.9 Hz, 564.3 Hz and 617.4 Hz. Uncertainties are unknown but those frequencies of micro-vibrations are expected to be constant during the mission.

PFS eigenmodes: The PFS eigenmodes are around 135 Hz and 160 Hz. Uncertainties are unknown but those frequencies of micro-vibrations are expected to be constant during the mission.

3. Results

Due to the stochastic character of the ghosts and especially their phase, few % of the PFS spectra in the archive, randomly distributed, present significant level of perturbations. In some lucky cases, the ghosts are absent but typical spectra contain few ghosts (Comolli and Saggin, 2010). We propose to illustrate our algorithm on the ORB0032, spectra No. 106 of PFS, recorded in particularly high level of disturbances. This spectrum contains several obvious ghosts (as shown by the arrows in Fig. 5).

We find that the optimum inversion is reached with a loop of $N = 2$, with special parameter for the first step using the filtered initialization ($\lambda_K = 50$) and then usual parameter ($\lambda_{Mars} = 0.001$, $\lambda_K = 1$) using the unfiltered spectra.

3.1. Mars spectra and kernel estimations obtained

For Mars spectra estimation, the final estimation of the signal $\hat{I}_{Mars}^{final}$ is presented in Figs. 4 and 5. This figure presents the raw spectra, our corrected spectra in comparison with a synthetic spectra $\hat{I}_{Mars}^{0}$ (see Section 2.2.2) and also the stack of 20 spectra. Our correction clearly removes the ghosts in the region at 1–1530 cm^{-1}, around 2700 cm^{-1}, around 3450 cm^{-1}, around 4150 cm^{-1} similar to the stacking method. The artifact at 2900 cm^{-1} persists due to pollution of hydrocarbons in the telescope (Giuranna et al., 2005b). In the 4000–5000 cm^{-1} domain, our method improves the signal in comparison to the

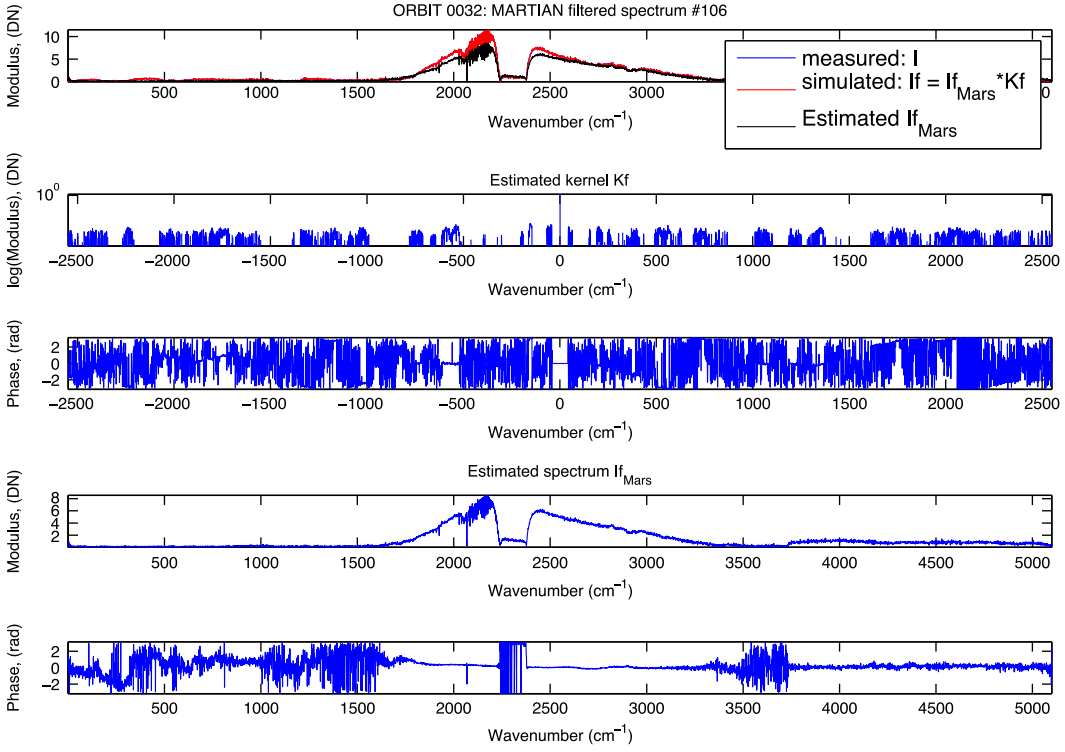

Fig. 4. Final results of the spectra ORB0032 #106: at the top: modulus of measured I_{PFS} (blue) simulated $\hat{I}_{PFS}^{final} = \hat{I}_{Mars}^{final} \star \hat{K}_{PFS}^{final}$ PFS spectra (red) and the estimated Martian spectra $\hat{I}_{Mars}^{final}$ (black); Lack of fit between I_{PFS} and $\hat{I}_{PFS}^{final}$ is 1.8×10^{-5}; in the middle: modulus (in log scale) and phase of the final estimated kernel $\hat{K}_{PFS}^{final}$; at the bottom: modulus and phase of the final estimated spectrum $\hat{I}_{Mars}^{final}$. (For interpretation of the references to color in this figure caption, the reader is referred to the web version of this paper.)

stacking method and partly correct the artificial decrease of the signal. The stacking clearly reduces the stochastic noise that is not removed with our correction.

Fig. 6 shows the evolution of the average spectra, when stacking 3, 5, 11 and 19 spectra. The plots clearly show that our method removes the ghosts contribution, already without stacking. On the contrary, the stacking methods require $\sim$ 10 spectra to remove this effect. The signal to noise ratio at small scale, estimated by the standard deviation in the 1–1530 cm^{-1}, is not significantly changed between both methods.

The stack of $\sim$10 spectra corresponds to $\sim$10 spots of around 7 km each, so that the spatial resolution can be improved by one order of magnitude. In terms of temporal resolution improvement, it depends mainly on the location due to the very irregular observation density.

3.2. Quality of the results

As illustrated in Fig. 4, the lack of fit between the real PFS spectra I_{PFS} and the simulated one from our final guesses $\hat{I}^{final}_{PFS} = \hat{I}^{final}_{Mars} \star \hat{K}^{final}_{PFS}$ is very small ($\sim 10^{-5}$), showing that the solution is compatible with the observation.

Our strategy is efficient to remove the norm in the 1–1530 cm^{-1} domain by a factor of $\sim$2 (the RMS is 0.0093 for the raw spectra and to 0.0042 for the corrected spectra). The only signal left in $\hat{I}^{final}_{Mars}$ seems to be very small scale at random, as expected (see Fig. 4). The theoretical value of noise standard deviation is about 0.1 using the estimated signal to noise ratio of about 100 in the 2000–2400 cm^{-1} (Giuranna et al., 2005b). The estimated noise standard deviation of corrected spectra is in agreement with this value (see Fig. 6). In order to estimate the efficiency of ghost removal, we measure the spectral energy in the 1–1530 cm^{-1} domain at scale larger than 50 cm^{-1} for corrected spectra in comparison to the measured spectra, assuming that the large scale features are only due to ghosts. We found that our correction for one single spectra remove 85% of the ghost energy, which is equivalent to the effect of stacking of 11 spectra.

The laser line modulated $\hat{I}^{final}_{LM}$ through filter, aliasing and vibration kernel $\hat{K}^{final}_{PFS}$ are compatible with the observation I_{LM} (see Fig. 7). The four mains peaks are estimated and also some smaller peaks. The distance is relatively small ($\sim$0.013).

The final kernel estimation $\hat{K}^{final}_{PFS}$ is close to the initial kernel guess $\hat{K}^{0}_{PFS} = \hat{K}^{approx}_{PFS}$ with a distance $\sim 10^{-5}$. As illustrated in Fig. 8, the main vibration frequencies estimated in $\hat{K}^{approx}_{PFS}$ are present in $\hat{K}^{final}_{PFS}$. The estimation of $\hat{K}^{approx}_{PFS}$ has been done under strong approximation. Especially the unconstrained amplitude may explain the differences. Also $\hat{K}^{final}_{PFS}$ presents a smooth signal due to the high frequencies filtering. Other methods without sparsity regularization does not succeed to get such a sparse kernel although we believe that the kernel is sparse due to limited vibrations in the mechanical environment of PFS onboard MEx (eigenmode of PFS, reaction wheels frequencies, inertia measurement unit dithering frequencies).

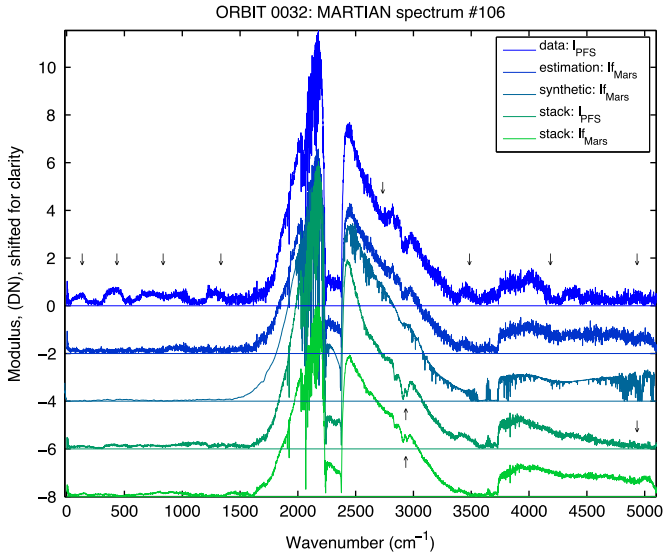

Fig. 5. Final results of the spectra ORB0032 #106 as compared with stacking and synthetic measurements, from top to bottom: (i) raw PFS measurements, all arrows represent ghosts artifacts, (ii) estimated spectra from our algorithm, (iii) synthetic measurement of PFS, (iv) stack of 11 PFS spectra, (v) stack of 11 estimated spectra from our algorithm. The arrow at 2900 cm^{-1} represents the mirror contamination by hydrocarbons, the arrow at 4900 cm^{-1} represents an artifact of abnormal small signal, probably due to ghosts.

4. Discussion and conclusion

We described the approximated direct problem and an algorithm able to correct for the mechanical vibration of the PFS instrument. For the first time, we show that it is possible to reduce significantly the ghosts from the observed signal from 3–5% of the total energy to 0.4–0.7%. We show that our estimation is coherent

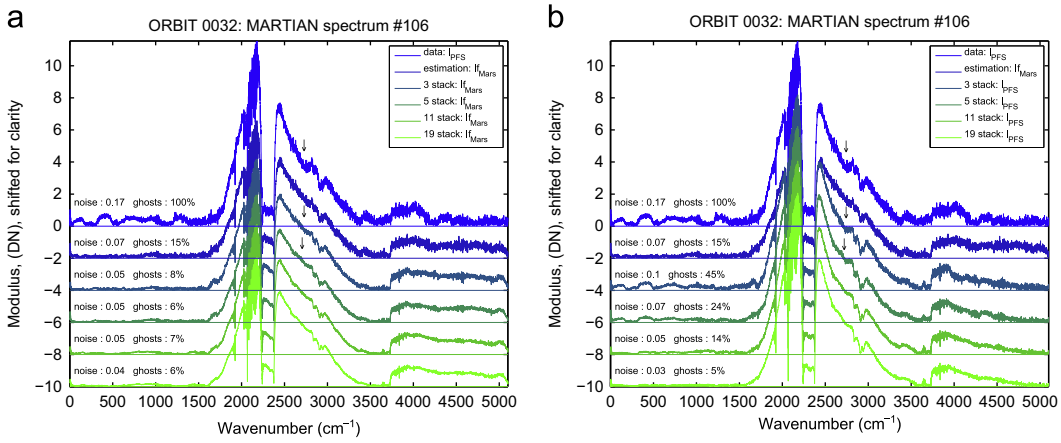

Fig. 6. Comparison of our correction versus the stacking method : Stacking of (a) corrected spectra from our method and (b) PFS spectra. Noise standard deviation from 1 to 1530 cm^{-1} is expressed for all spectra. Fraction of energy due to ghosts, relative to the raw PFS spectra in 1–1530 cm^{-1}, is also written for all spectra. Arrows at 2700 cm^{-1} represent significant difference in the signal domain due to ghosts, that persists for stacking of at least 5 PFS spectra but well corrected by our method.

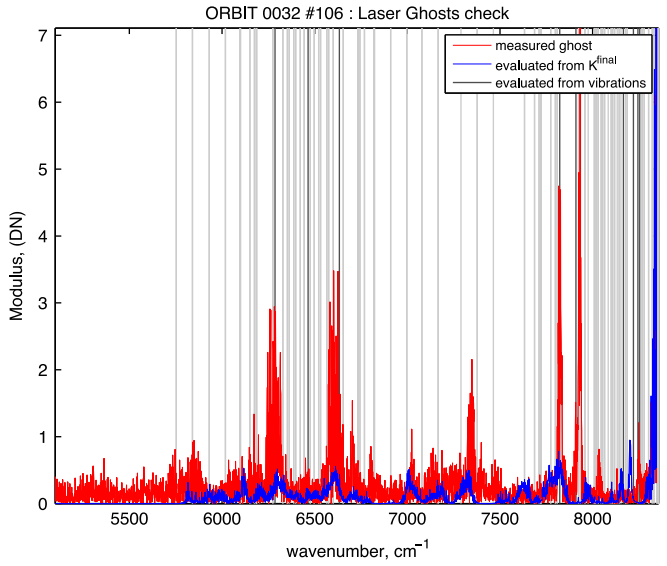

Fig. 7. Modulus of the simulated laser line modulated $\hat{I}_{LM}^{final}$ through filter, aliasing and vibration kernel $\hat{K}_{PFS}^{final}$ (blue) and the observation I_{LM} (red). The lack of fit is 0.0270. (For interpretation of the references to color in this figure caption, the reader is referred to the web version of this paper.)

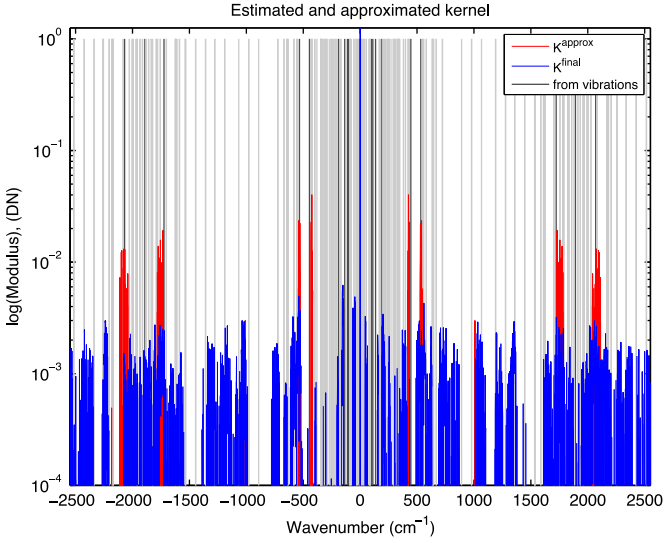

Fig. 8. Modulus in log scale of the vibration kernel $\hat{K}_{PFS}^{final}$ (blue line), the approximated kernel $\hat{K}_{PFS}^{approx}$ (red line) and the reaction wheels vibration (dark grey line), and the combination of reaction wheels (light grey line). The lack of fit is 3.2×10^{-4}. (For interpretation of the references to color in this figure caption, the reader is referred to the web version of this paper.)

using three quantities: ghosts in the signal domain, laser line ghosts, distance to approximated kernel. Thus the global shape of PFS SWC spectra can be corrected with our algorithm, allowing to better estimate temperature, and thermal profile on each PFS measurement, improving the few % of spectra with high χ^2 that could not be processed with current calibration (Grassi et al., 2005). Also, our correction may avoid the continuum removal step in the minor species retrieval (Sindoni et al., 2011). When the signal to noise ratio is high enough, our correction will also reduce the stacking procedure.

In the future, we would like to propose an algorithm to correct the complete archive that would require efficient algorithm, timesaving implementation, and fully automatic procedure. Also, new correction procedure must be developed to treat the whole orbits currently available (6405 at the date of writing).

In order to correct any shaked FTS, semi-blind deconvolution is possible, knowing $\hat{I}_{Mars}^{0}$ (but without knowing $\hat{K}_{PFS}^{approx}$ from the "laser line domain") so that the "signal domain" only is required. Thus, any techniques of optical path measurement (laser line, mechanical, etc.) can be corrected with our technique. Nevertheless, the independent estimation of the kernel $\hat{K}_{PFS}^{approx}$ significantly improves the convergence of the algorithm. The only limitation to apply this method on other instruments is about the convolution equation. Convolution is true if the signal from the planet I_{Mars} has a significantly reduced wavenumber domain (as stated in Eqs. (1)–(3)).

Acknowledgments

We thank Ali Mohammad-Djafari for fruitful discussions. We acknowledge support from the "Institut National des Sciences de l'Univers" (INSU), the "Centre National de la Recherche Scientifique" (CNRS) and "Centre National d'Etude Spatiale" (CNES) and through the "Programme National de Planétologie". We also thank "European Space Agency" (ESA) for providing the reaction wheels speed of MEx. We finally thank two anonymous reviewers for their comments.

References

Beck, A., Teboulle, M., 2009. A fast iterative shrinkage-thresholding algorithm for linear inverse problems. SIAM J. Imaging Sci. 2 (1), 183–202.

Chen, S., Donoho, D., Saunders, M., 1998. Atomic decomposition by basis pursuit. SIAM J. Sci. Comput. 20 (1), 33–61.

Comolli, L., Saggin, B., 2005. Evaluation of the sensitivity to mechanical vibrations of an IR Fourier spectrometer. Rev. Sci. Instrum. 76 (December (12)), 123112–-123118, URL http://dx.doi.org/10.1063/1.2149009.

Comolli, L., Saggin, B., 2010. Analysis of disturbances in the planetary Fourier spectrometer through numerical modeling. Planet. Space Sci. 58 (April (5)), 864–874, URL ⟨http://www.sciencedirect.com/science/article/B6V6T-4Y9CF-BX-2/2/950f692b594101f9b0558dae213e3fc1⟩.

Formisano, V., Angrilli, F., Arnold, G., Atreya, S., Bianchini, G., Biondi, D., Blanco, A., Blecka, M., Coradini, A., Colangeli, L., Ekonomov, A., Esposito, F., Fonti, S., Giuranna, M., Grassi, D., Gnedykh, V., Grigoriev, A., Hansen, G., Hirsh, H., Khatuntsev, I., Kiselev, A., Ignatiev, N., Jurewicz, A., Lellouch, E., Moreno, Lopez, 2005. The planetary Fourier spectrometer (pfs) onboard the european mars express mission. Planet. Space Sci. 53 (August (10)), 963–974, URL ⟨http://www.sciencedirect.com/science/article/B6V6T-4G94HR4-2/2/c10c243741b6a0444b7d58665e9ec980⟩.

Giuranna, M., Formisano, V., Biondi, D., Ekonomov, A., Fonti, S., Grassi, D., Hirsch, H., Khatuntsev, I., Ignatiev, N., Malgoska, M., Mattana, A., Maturilli, A., Mencarelli, E., Nespoli, F., Orfei, R., Orleanski, P., Piccioni, G., Rataj, M., Saggin, B., Zasova, L., 2005a. Calibration of the planetary Fourier spectrometer long wavelength channel. Planet. Space Sci. 53 (August (10)), 993–1007, URL ⟨http://www.sciencedirect.com/science/article/B6V6T-4GCX0HK-1/2/9d8e4485b4eb45a54082fef03d4718a5⟩.

Giuranna, M., Formisano, V., Biondi, D., Ekonomov, A., Fonti, S., Grassi, D., Hirsch, H., Khatuntsev, I., Ignatiev, N., Michalska, M., Mattana, A., Maturilli, A., Moshkin, B., Mencarelli, E., Nespoli, F., Orfei, R., Orleanski, P., Piccioni, G., Rataj, M., Saggin, B., Zasova, L., 2005b. Calibration of the planetary Fourier spectrometer short wavelength channel. Planet. Space Sci. 53 (August (10)), 975–991, URL ⟨http://www.sciencedirect.com/science/article/B6V6T-4GCX1K5-2/2/a2f8e53774cbfb604eedcff6055edf4c⟩.

Grassi, D., Ignatiev, N., Zasova, L., Maturilli, A., Formisano, V., Bianchini, G., Giuranna, M., 2005. Methods for the analysis of data from the planetary Fourier spectrometer on the mars express mission. Planet. Space Sci. 53 (August (10)), 1017–1034, URL ⟨http://www.sciencedirect.com/science/article/pii/S0032063305000693⟩.

Idier, J. (Ed.), 2008. Bayesian Approach to Inverse Problems. ISTE Ltd and John Wiley & Sons Inc.

Saggin, B., Comolli, L., Formisano, V., 2007. Mechanical disturbances in Fourier spectrometers. Appl. Opt. 46 (August (22)), 5248–5256, URL ⟨http://ao.osa.org/abstract.cfm?URI=ao-46-22-5248⟩.

Shatalina, I., Schmidt, F., Saggin, B., Gac, N., Kowalski, M., Giuranna, M., Nhean, S. Analytical expression of combined microvibrations effects on Fourier spectrometer. Aerospace Sci. Technol., submitted for publication.

Sindoni, G., Formisano, V., Geminale, A., 2011. Observations of water vapour and carbon monoxide in the martian atmosphere with the SWC of PFS/MEX. Planet. Space Sci. 59 (February (2–3)), 149–162, URL ⟨http://www.sciencedirect.com/science/article/B6V6T-51TGG5K-1/2/fdab0daa9bc5411b1c90cafa0ca13bae⟩.

Tibshirani, R., 1996. Regression shrinkage and selection via the lasso. J. R. Stat. Soc. Ser. B 58 (1), 267–288.